

pubs.acs.org/JPCA Article

# Conformer-Specific Spectroscopy and IR-Induced Isomerization of a Model $\gamma$ -Peptide: Ac- $\gamma^4$ -Phe-NHMe

Joshua L. Fischer, Karl N. Blodgett, Christopher P. Harrilal, Patrick S. Walsh, Zachary S. Davis, Sunglim Choi, Soo Hyuk Choi, and Timothy S. Zwier\*



Cite This: J. Phys. Chem. A 2022, 126, 1837–1847



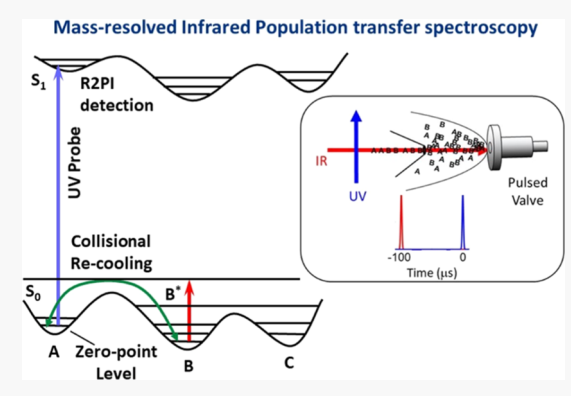
**ACCESS** I

III Metrics & More

Article Recommendations

s Supporting Information

**ABSTRACT:** Single-conformation IR and UV spectroscopy of the prototypical capped  $\gamma$ -peptide Ac- $\gamma^4$ -Phe-NHMe ( $\gamma^4$ F) was carried out under jet-cooled conditions in the gas phase in order to understand its innate conformational preferences in the absence of a solvent. We obtained conformer-specific IR and UV spectra and compared the results with calculations to make assignments and explore the differences between the  $\gamma^2$ -and  $\gamma^4$ -substituted molecules. We found four conformers of  $\gamma^4$ F in our experiment. Three conformers form nine-membered hydrogen-bonded rings (C9) enclosed by an NH···O=C H-bond but differing in their phenyl ring positions (a, g+, and g-). The fourth conformer forms a strained seven-membered hydrogen-bonded ring in which the amide groups lie in a nominally anti-parallel arrangement stacked on top of one another (labeled S7). This conformer is a close analogue of the amide-stacked conformer (S) found previously in  $\gamma^2$ F, in which the Phe side chain is substituted at the  $\gamma^2$ 



position, Ac- $\gamma$ 2-Phe-NHMe (*J. Am. Chem. Soc.* **2009**, *131*, 14243–14245). IR population transfer spectroscopy was used to determine the fractional abundances of the  $\gamma^4$ F conformers in the expansion. A combination of force field and density functional theory calculations is used to map out the conformational potential energy surfaces for  $\gamma^4$ F and compare it with its  $\gamma^2$ F counterpart. Based on this analysis, the phenyl ring prefers to take up structures that facilitate NH··· $\pi$  interactions in  $\gamma^4$ F or avoid phenyl interactions with the C=O group in  $\gamma^2$ F. The disconnectivity graph for  $\gamma^4$ F reveals separate basins associated with the C9 and amide-stacked conformational families, which are separated by a barrier of about 42 kJ/mol. The overall shape of the potential energy surface bears a resemblance to peptides and proteins that have a misfolding pathway that competes with the formation of the native structure.

# 1. INTRODUCTION

In most peptides and proteins, hydrogen bonding plays an integral role in directing the molecule's secondary and tertiary structures, and therefore potential bioactivity, creating an imperative demand to understand the propensities driving these interactions. 1-4 Synthetic foldamers are oligomers designed to display discrete folding propensities determined by the chemist, ideally allowing control over bioactivity.<sup>5</sup> To that end, synthetic chemists have endeavored to create designer peptidomimetics that allow control over the formation of hydrogen bonds to create tailor-made secondary and tertiary structures.<sup>6,7</sup> Introducing more flexibility in both the peptide substituents and substitution location allows more control over folding preferences, creating an interest in peptides with extended backbones, such as in  $\beta$ - and  $\gamma$ peptides, which extend the peptide backbone between the Nand C-terminus by one and two carbon atoms, respectively, with respect to naturally occurring  $\alpha$ -peptides.<sup>8</sup>

Interrogating the conformations adopted by synthetic foldamers is traditionally done in the solid and liquid phases

by X-ray crystallography and NMR spectroscopy. <sup>9–11</sup> However, gas-phase spectroscopic methods provide a unique opportunity to study the conformations and unique spectroscopic signatures of molecules at a high resolution and free from intermolecular interactions. <sup>12–18</sup> In a gas-phase supersonic expansion, the molecules are cooled into their conformational zero-point levels, enabling interrogation of their innate conformational preferences by comparing the experimental spectra with calculated structures and spectra of the conformational minima of the bare molecule.

In the present work, we carry out a detailed study of the conformational preferences of the model capped  $\gamma$ -peptide Ac $\gamma$ 4-Phe-NHMe ( $\gamma$ <sup>4</sup>F) shown in Figure 1. By comparison of the

Received: January 7, 2022 Revised: February 23, 2022 Published: March 11, 2022





\* 
$$\begin{pmatrix} 4 & 2 \\ \\ 1 & 3 \end{pmatrix}$$
  $\begin{pmatrix} 2 \\ \\ 0 \end{pmatrix}$   $\begin{pmatrix} 0 \\ \\ 0 \end{pmatrix}$   $\begin{pmatrix} 0 \\ \\ 0 \end{pmatrix}$   $\begin{pmatrix} 0 \\ \\ 1 \end{pmatrix}$   $\begin{pmatrix} 0 \\ \\ 0 \end{pmatrix}$   $\begin{pmatrix} 0 \\ \\ 1 \end{pmatrix}$   $\begin{pmatrix} 0$ 

Figure 1. Scheme depicting the numbering assigned to the positions of substitution along the peptide backbone (top), and the dihedral angles of relevance in  $\gamma^4F$  (bottom). The phenyl rotor dihedral is highlighted in red.

conformer-specific IR spectra with calculation, we assign the spectra to particular conformational isomers, providing insights into the structural properties that drive the conformational preference. We also identify unique spectroscopic signatures of these interactions using double-resonance methods. <sup>19</sup>

This work is a natural extension of previous studies by our group of Ac- $\gamma^2$ -Phe-NHMe ( $\gamma^2$ F), which differs in the position of substitution of the phenylalanine side chain on the  $\gamma$ -peptide backbone. 17,20 In that work, we observed for the first time a conformation that was engaged in amide stacking: a fascinating interaction in which two amide groups stack on top of one another in anti-parallel fashion. The stacked amide groups interact via a combination of favorable electrostatic and dispersive interactions, with no H-bond between them. The spectroscopic signature of amide stacking is obvious in the NH-stretch region, where the two NH-stretch fundamentals associated with the stacking pair appear above 3450 cm<sup>-1</sup> and where free amide NH groups absorb. In  $\gamma^2$ F, the stacked conformer is present in combination with the two conformers that form a hydrogen bond between the N-terminal C=O and H from the protecting NHMe group, forming a ninemembered H-bonded ring (labeled "C9"). Additionally, the relative populations of the conformers present in the expansion were measured, showing that amide stacking accounted for about 20% of the population, a surprisingly high abundance considering the amide stack has no hydrogen bonds.

In order to assess the characteristics that facilitated amide stacking, James et al. studied a set of three derivatives of  $\gamma^2$ F that tipped the balance of conformations toward all amide stacked (in Ac- $\gamma^2$ -Phe-NMe<sub>2</sub>), all C9 (Ac- $\gamma^2$ -Phe-NH-iPr), and all C7 H-bonded conformations (in a cyclically constrained gabapentin derivative). Finally, James et al. also studied a series of extended  $\gamma^2$ -dipeptides to see if amide stacking survived in longer peptides but found no experimental evidence for them.

Given the sensitive relationship of the conformational preferences of  $\gamma$ -peptides with their structures,  $^{21}$  it is natural to ask how the presence and nature of amide stacking are affected by moving the position of substitution along the  $\gamma$ -peptide backbone. This is the task we take up here in our studies of  $\gamma^4 F$ , which has the phenylalanine (Phe, F) side chain positioned in the 4-position of the  $\gamma$ -peptide backbone immediately adjacent to the N-terminal amide NH. The choice of substitution at the 4-position is motivated by results in solution that suggested that  $\gamma^4$ -residues would form specific

secondary structures more readily than their  $\gamma^2$  counterparts.  $^{22,23}$ 

#### 2. METHODS

**2.1. Experimental.** 2.1.1. Synthesis and Sample Handling. Ac- $\gamma^4$ -Phe-NHMe ( $\gamma^4$ F) was synthesized using the procedure described in the Supporting Information. The sample was dried using a lyophilizer to remove water from the solid, allowing spectra of the  $\gamma^4$ F monomer free from interference from  $H_2O$  complexes to be taken. Solid dry  $\gamma^4F$ was wrapped in glass wool and placed inside of a glass insert housed inside a stainless-steel sample holder located immediately before a pulsed valve (Parker General Valve, Series 9) filled with a neon carrier gas (5 bar). The dried sample was then heated to 180-185 °C by a heating rope and expanded into vacuum, generating a cold molecular beam that provided collisional cooling of the sample to its zero-point vibrational levels. The resulting expansion was skimmed through a ~2 mm dia. skimmer into the extraction region of a Wiley-McLaren time-of-flight (TOF) mass spectrometer.

2.1.2. Spectroscopic Methods. The output of a Nd:YAG (Continuum, Surelite II, 20 Hz) pumped dye laser (NarrowScan, Coumarin 540A) was frequency doubled and introduced into the chamber orthogonally to the molecular beam as it passed through the extraction region of the TOF. Ions are generated by resonant two-photon ionization (R2PI), and then extracted into the TOF tube and detected using an MCP detector. The ion intensity at an arrival time specific to the mass of the target analyte was monitored as a function of the laser frequency to generate UV spectra.

The output of a Nd:YAG (Continuum, Surelite III, 10 Hz) was used to pump an optical parametric oscillator/amplifier stage (LaserVision) which outputs IR radiation in the NH-stretch region. In the present work, IR radiation was introduced anti-parallel to the molecular beam such that the IR light passed through the skimmer and intersected the pulsed valve at the valve orifice, enabling molecules all along the expansion axis to be excited with IR radiation.

Double resonance methods were used to generate conformer-specific IR and UV spectra. These methods utilize 20/10 Hz repetition rates of the UV and IR lasers, respectively. The delay between UV and IR light pulses controls how far the interrogated molecules travel from the pulsed valve toward the TOF extraction region before interacting with the IR radiation. In resonant ion-dip infrared spectroscopy (RIDIRS), the UV laser is fixed at the frequency of a conformer-specific transition, producing a steady-state ion signal due to that conformer. The frequency of the IR laser is then scanned with the IR preceding the UV laser by  $\sim 60 \mu s$ , which is approximately the time it takes for IR-excited molecules to travel from the skimmer to the extraction region of the TOF. Since this interrogation point is under collision-free conditions, when the IR laser frequency is resonant with a vibrational transition of a particular conformer, the population is removed from its zero-point vibrational level by the IR source. The ion signal from  $\gamma^4$ F has its intensity modulated every other UV laser pulse by the absorption induced by the IR laser. Because the UV laser generates a signal only from one conformer, the ion signal will only be depleted when the IR and UV laser are on transitions that belong to the same conformer, and a conformer-specific IR spectrum is generated by taking the difference of the IR-on/ IR-off ion signals. Since the IR laser fills the skimmer orifice, all molecules entering the extraction region of the TOFMS are

exposed to the IR laser pulse, leading to IR depletion spectra with an excellent signal-to-noise ratio.

IR ion gain spectroscopy (IRIGS) uses the same timings and alignment of lasers as RIDIRS, but in this case, the wavelength of the UV laser is fixed just to the red of the resonant transitions due to the conformers of  $\gamma^4 F$ . When the IR laser is scanned over the transition of any conformer, vibrationally excited conformers are produced that result in spectral broadening of the UV transition. This non-conformer-specific broadening will cause gain in the ion signal produced by the UV laser, resulting in an IR spectrum that is not conformer specific but contains IR transitions for all the conformers present in the expansion.

IR-UV hole-burning (IR-UV HB) provides a means of recording conformer-specific UV spectra. It uses the same laser alignment and timings as the other double resonance schemes but simply swaps which laser is fixed (IR) and which is tuned (UV). By choosing a fixed wavelength for the IR laser, which selectively excites an IR transition of a single conformer, A, the difference in the ion signal with or without the IR laser produces an ion signal whose intensity is modulated only when the UV frequency and IR frequency both excite transitions due to the conformer A, thereby generating its UV spectrum free from interference from other conformers present in the expansion.

One of the goals for many conformation-specific studies is to determine the fractional abundances  $F_i$  of the conformers, which cannot be obtained simply from the R2PI scan because of unknown differences in the Franck–Condon factors or photoionization cross-sections of the conformers. Infrared population transfer (IRPT) spectroscopy provides a means for obtaining the set of fractional abundances  $F_i$ .

In its present implementation (Figure 2), the method uses the same laser alignment as RIDIRS but varies the timing between the IR and UV lasers so that the UV laser interrogates molecules that were excited by the IR laser just outside the pulsed valve nozzle exit, where the buffer gas number density is sufficiently high to re-cool the IR-excited molecules prior to interrogation downstream. The IR laser frequency is set to a

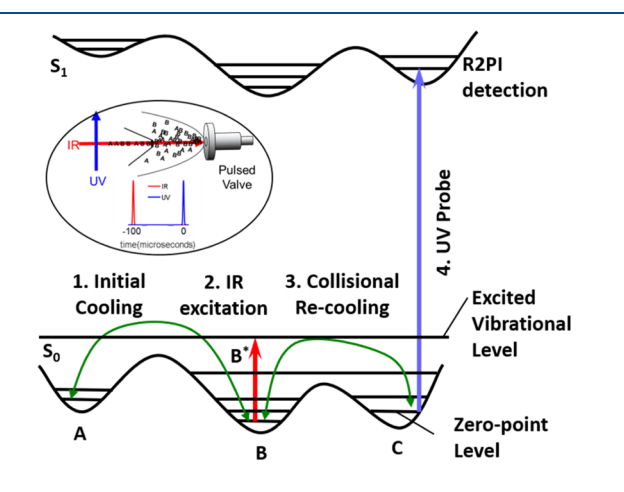


Figure 2. Schematic energy level diagram for IRPT spectroscopy. Inset: spatial configuration of the lasers, with the IR laser counterpropagating the molecular beam, with the IR–UV delay set to interrogate molecules excited by the IR within a few mm of the nozzle orifice where collisional cooling is complete, but many collisions occur following IR excitation to re-cool the IR excited molecules. See the text for further discussion.

conformer-specific transition, exciting molecules early in the expansion such that they can then be re-cooled by subsequent collisions in the expanding gas. Assuming that the IR photon provides the molecule with enough energy to overcome isomerization barriers and the cooling rate allows sufficient time for isomerization to occur, the population of the conformers initially vibrationally excited will be depleted as they isomerize, while that of conformational minima into which the molecules isomerize will grow. If no new conformers are populated, there is no net change in the total population of the molecule following re-cooling but only in the relative populations of the individual conformers. This criterion on the zero net-change in conformer population at all IR-excitation frequencies enables the fractional abundances  $F_i$  of each conformer i to be determined from a set of IRPT scans; that is  $^{25,26}$ 

$$\Delta N_{\text{tot}} = \sum_{i} F_{i}^{*} I_{i}^{\text{PT}}(\tilde{\nu}) = 0$$
(1)

where  $I_i^{\rm PT}(\tilde{\nu})$  is the intensity of the IRPT scan of conformer i, recorded as a change in fractional abundance as a function of wavenumber,  $\tilde{\nu}$ . An in-house script was used to find the best-fit fractional abundances by systematically stepping each  $F_i$  between 0 and 1 in values of 0.01 while taking the weighted sum of all IRPT spectra. The best-fit values of  $F_i$  are those which have the smallest root-mean-square deviation from zero when summed over all frequencies.

Finally, UV spectra showing the gain and depletion of the population were also acquired. These spectra are called IR—UV hole-filling (IR—UV HF) spectra and simply involve swapping the tuned and fixed wavelengths for IR and UV under hole-filling conditions. These spectra give an easy-to-interpret measure of how conformers redistribute their populations at specific IR wavelengths. Furthermore, sharp gain transitions provide an indication of successful re-cooling after IR excitation.

2.1.3. Computational Methods. A conformational search of the potential energy surface using the OPLS3 molecular mechanics force field<sup>28</sup> was carried out using Monte Carlo methods to vary the dihedral angles of the  $\gamma$ -peptide with MacroModel<sup>29</sup> included in the Maestro software suite, allowing a population of low-energy conformers to be identified. The lowest 100 energy structures were further optimized with density functional theory (DFT) using either the B3LYP functional<sup>30</sup> with Grimme's D3(BJ) dispersion correction  $^{31,32}$  or the M05-2X functional,  $^{33}$  both with the 6-31+G(d) basis set using Gaussian 16.  $^{34}$  It was found that B3LYP-GD3(BJ) predicted relative energies that were consistent with the experimental fractional abundances but provided unsatisfactory predictions of vibrational frequencies in cases where dispersive interactions played a significant role (e.g., NH $\cdots\pi$ ). Accordingly, when comparing energies to relative populations, B3LYP-GD3(BJ) was used, while M05-2X results were employed to obtain scaled harmonic frequencies and IR intensities for comparison with the experimental IR spectra. Dihedral scans were also carried out using Gaussian 16 with the B3LYP-GD3(BJ). The harmonic vibrational frequencies were scaled by factors which account for anharmonicity. The frequencies of the NH-stretch vibrations calculated using the M05-2X functional were scaled by 0.940 for comparison with the experiment.

To gain a deeper understanding of the conformational energy landscape, we used the suite of programs developed by

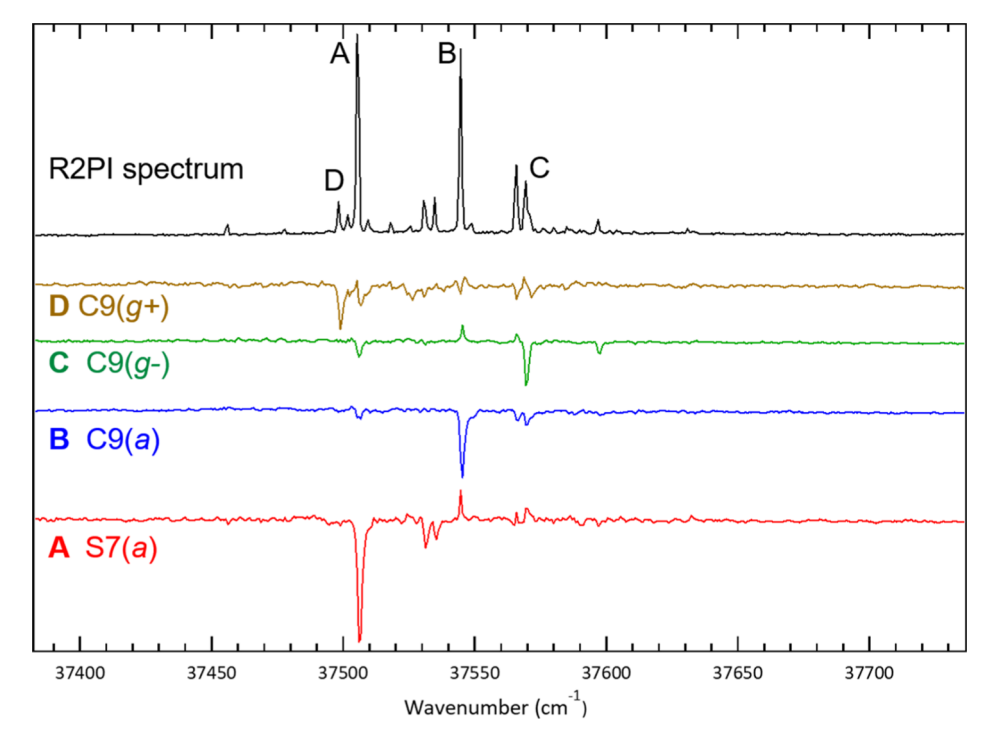


Figure 3. R2PI (top, black) and IR–UV hole-burning spectra (bottom, colored) taken for conformers A–D of  $\gamma^4$ F in the  $S_0$ – $S_1$  origin region of the phenyl UV chromophore. The small departures from zero in A–D are artifacts due to incomplete subtraction of the difference signal when going through transitions with large intensity.

Evans and Wales<sup>35</sup> to generate disconnectivity graphs for  $\gamma^2 F$  and  $\gamma^4 F$ . Disconnectivity graphs provide a visual summary of the energy minima and the transition states that separate them. The minima are located at the ends of each branch, while the transition states are grouped into energy-tiered nodal points connecting groups of minima below them. The AMBER\* force field<sup>36</sup> was employed to locate the minima and transition states. In the present case, this force field does a surprisingly good job of reproducing the relative energies of low-lying minima from the DFT calculations.

# 3. RESULTS AND ANALYSIS

**3.1. Nomenclature.** Figure 1a shows the numbering system used to specify the position where backbone substitution occurs in  $\gamma$ -peptides, while Figure 1b shows the additional dihedral angles that must be specified in  $\gamma$ -peptides in addition to the  $\phi/\psi$  angles found in naturally occurring  $\alpha$ -amino acids. The first dihedral (C(3)–C(4)) following the  $\phi$  Ramachandran angle is denoted  $\theta_1$ , while the C(2)–C(3) dihedral angle is  $\theta_2$ . Intramolecular hydrogen bonds are labeled "Cn" to denote the size of the H-bonded ring closed by "n" atoms in the ring (e.g., C9 for a nine-membered ring).

The position of the phenyl ring relative to the backbone also plays an important role in distinguishing conformers. Accordingly, the phenyl ring position will be given in parentheses following the conformer label, with  $g\pm$  denoting gauche ( $g+\approx+60^\circ$ ,  $g-\approx-60^\circ$ ) and "a" for anti (a  $\sim180^\circ$ ) about the dihedral shown in red in Figure 1. Along the backbone, dihedral angles are defined starting with the atom closest to the N-terminus.

3.2. Spectroscopy of  $\gamma^4$ F Monomer and Conformational Assignments. 3.2.1. R2PI Spectrum. The R2PI spectrum in the S<sub>0</sub>-S<sub>1</sub> origin region of  $\gamma^4$ F shown in the top scan of Figure 3 was taken while monitoring the parent mass

channel (m/z 248.2). Initial scans (shown in Figure S1) displayed a more highly congested spectrum than anticipated. Upon taking RIDIR spectra of some of the transitions at the blue end of the spectrum, we identified some of them as being due to  $\gamma^4 F - H_2 O$  complexes due to the presence of residual water in the sample. The fact that they show up in the  $[\gamma^4 F]^+$  mass channel (m/z 248.2) indicates that the complex was fragmenting with high efficiency by loss of  $H_2 O$  following photoionization, as has been observed in certain water-containing clusters in the past.  $^{37-39}$  Upon drying the sample, the transitions due to the  $\gamma^4 F - H_2 O$  complex all but disappeared from the parent mass channel, leaving the spectrum shown in Figure 1 ascribable to the  $\gamma^4 F$  monomer.

TOF mass spectra recorded with the R2PI laser fixed on representative vibronic transitions of the  $\gamma^4$ F monomer exhibited, in addition to the parent mass peak, a strong fragment signal at m/z 157.1 ascribable to the loss of the benzyl radical (91 amu) from the parent ion (Figure S2). Furthermore, the R2PI spectra of the parent and fragment show differences in the relative intensities of UV transitions due to different conformers, indicating that certain conformers fragment more readily than others. Table 1 summarizes the fragmentation ratio for each of the conformational isomers identified in the spectrum. The high fragmentation yield

Table 1. Ratio of the Parent (Par), Fragment (Frag), and Sum of Both Parent and Fragment (Sum) Ion Intensities to Each Other for the Respective Identified Conformers A-D Origin Peaks Maximum Intensity

	A	В	С	D
parent/Sum	0.46	0.42	0.50	0.54
fragment/Sum	0.54	0.58	0.50	0.46
Int(Frag)/Int(parent)	1.14	1.38	1.00	0.85

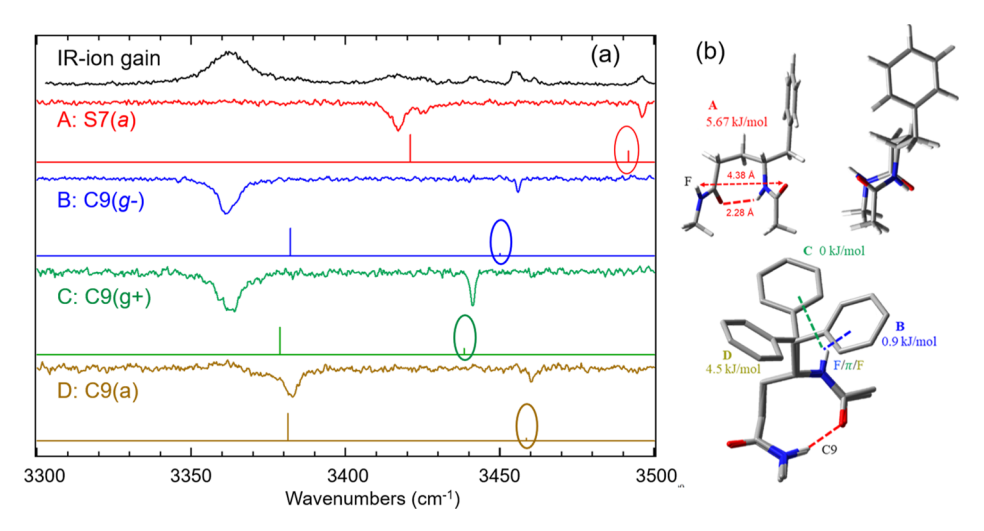


Figure 4. (a) IR ion-gain spectrum of  $\gamma^4F$  (top, black) is plotted above the conformer-specific RIDIRS scans of the four observed conformers A–D of  $\gamma^4F$  in the amide NH-stretch region (colored). The corresponding calculated best-fit spectra are plotted below each colored RIDIR spectrum. (b) Assigned conformers of  $\gamma^4F$ . A topdown and side profile of conformer A is shown to illustrate the S7 conformation with its distorted amide stacking. Note that the three C9 conformers share nearly identical backbone dihedral angles and have been overlaid to illustrate this similarity. The color-coded letter next to each structure associates the assigned conformer to its corresponding RIDIR spectrum and its calculated relative energy in kJ/mol.

distributes the parent absorption over two mass channels, so the sum of both channels is used to generate the UV spectrum for the monomer shown in Figure S3.

3.2.2. Single Conformation IR and UV Spectra. The IR spectra of the four unique conformers identified through RIDIR/IR–UV HB spectroscopy are shown in Figure 4. Each single-conformer IR spectrum contains two NH-stretch transitions, as anticipated by the presence of two amide groups in  $\gamma^4$ F. Figure 4 also displays an IR-ion gain spectrum (top, black), which is not conformer-specific but instead shows the transitions of all the conformers of  $\gamma^4$ F present in the expansion.

Below the IRIG spectrum are the conformer-specific RIDIR spectra, as well as the best-fit stick spectra of the assigned conformers, calculated using the M05-2X functional. A comparison of the transitions in the IRIG spectrum with the four RIDIR spectra confirms that these four conformers account for all major peaks in the IRIG scan.

The RIDIR spectrum of conformer A, shown in red, is compared with the best-fit calculated spectrum below it. The calculated vibrational frequencies and IR intensities of a broader range of conformational structures are compared with the experiment in Figure S4. The experimental spectrum for conformer A contains a broad, intense transition centered at 3416 cm<sup>-1</sup> with a shoulder at 3425 cm<sup>-1</sup>. We assign the main transition to a strained C7 H-bond (which we label as S7) between the N-terminal NH group and the C-terminal carbonyl oxygen. The sharp, weak transition at 3496 cm<sup>-1</sup> is the free NH stretch of the NHMe group. It is located about 35 cm<sup>-1</sup> higher in frequency than the free NH-stretch fundamentals of amides attached to secondary carbon atoms, 12,40 and therefore is a spectroscopic signature that the NHMe group is free. We tentatively assign the shoulder at 3425 cm<sup>-1</sup> to the overtone of the H-bonded C=O stretch (with a calculated harmonic frequency of  $1728 \times 2 = 3456$ cm<sup>-1</sup>) showing up as a result of Fermi resonance with the NHstretch fundamental at 3416 cm<sup>-1</sup>.

Conformer A is assigned to the S7(a) structure shown from two viewpoints in Figure 4b. The phenyl ring is in the anti position with an N–C–C–C(ph) dihedral of  $\sim 180^\circ$ . It is noteworthy that the S7 hydrogen bond is highly strained having a  $\angle$ COH angle of 88° and a direction of approach in which the amide groups are nearly stacked but distorted from an anti-parallel arrangement in order to facilitate formation of the S7 H-bond. Indeed, the NH group involved in the H-bond has an NH···O=C distance of 2.28 Å compared to the corresponding NH···O=C distance of 4.38 Å for the free NH–Me group is in the opposite amide plane.

The NH-stretch transitions are highly sensitive to this distortion away from planar stacked ones. The NH-stretch fundamentals of the amide-stacked conformer of  $\gamma^2 F^{17,20}$  occur at 3469 and 3480 cm $^{-1}$  while those in S7(a) of  $\gamma^4 F$  are at 3416 and 3496 cm $^{-1}$ . The zero-point corrected energy of the S7(a) conformer is 6.3 kJ/mol above the global minimum (the sixth-lowest energy structure), which is surprisingly high in energy for a conformer that appears to be in relatively high abundance based on the peak intensities of the electronic spectrum. However, since differences in Franck—Condon factors, excited-state lifetimes, and photoionization cross-sections can all affect the relative intensities in the R2PI spectrum, this motivates experiments that measure the fractional abundance without relying on the intensities in the R2PI spectrum.

The RIDIR spectra of conformers B, C, and D in the NH-stretch region are all shown above their corresponding best-fit stick spectra in Figure 4a. The best-fit calculations all show good agreement with the experimental spectra, leading to confident structural assignments. The three spectra are strikingly similar, showing a broad peak in the  $\sim 3360-3380$  cm<sup>-1</sup> region characteristic of a C9 H-bond and a free or nearly free amide NH stretch at 3440-3460 cm<sup>-1</sup>. These latter transitions shift by characteristic amounts that are captured by the calculations.

Figure 4b shows an overlay of the three assigned conformers, which all possess a C9 H-bond but differ in the position of the phenyl ring. The hydrogen-bonded transition for conformer B is centered at  $\sim 3361~{\rm cm}^{-1}$ , for conformer C at 3363 cm<sup>-1</sup>, and for conformer D at 3382 cm<sup>-1</sup> and is assignable to the C-terminal amide NH being hydrogen bound to the N-terminal

carbonyl oxygen. The remaining NH-stretch transitions for conformer B and conformer D are found at 3455 and 3460 cm<sup>-1</sup>, respectively, both assignable as free NH stretches of the N-terminal amide NH group. Their N–C–C–C(ph) dihedral angles of  $-52^{\circ}$  for conformer B and  $-172^{\circ}$  for conformer D lead to their assignments as C9(g–) and C9(a), respectively. The corresponding transition in conformer C appears at 3441 cm<sup>-1</sup> with increased relative intensity, characteristic of an NH– $\pi$  interaction, and is assigned as C9(g+). This conformer is calculated to be the zero-point-corrected global minimum in energy, with conformers B and D 0.9 and 4.5 kJ/mol less stable, respectively.

The relative frequencies of the  $S_0-S_1$  origins in the R2PI spectrum are consistent with these assignments. Conformer D[C9(a)] has the same phenyl ring orientation as conformer A[S7(a)] and has an  $S_0-S_1$  origin shifted only  $-7~{\rm cm}^{-1}$  from A. Conformer C[C9(g+)] possesses an NH  $\pi$  H-bond, which is known to shift the  $S_0-S_1$  origin of the phenyl ring to the blue,  $^{37-39}$  in this case by +64 cm<sup>-1</sup> relative to that of A. Finally, conformer B[C9(g-)] is between these two extremes since it is also positioned to experience a weak  $\pi$  H-bonding interaction.

There are two other low-energy conformers predicted by our conformational search, both of which are phenyl rotamers of conformer A[S7(a)]. Given the positioning of the phenyl ring in these two rotamers, we anticipate that they would appear near the electronic origin of A, having no possibility of  $\pi$  H-bonding. If present, they may contribute to congestion near the origin of conformer A in the R2PI spectrum (Figure 3).

Having determined the conformer-specific IR spectra, we pick unique IR absorption frequencies to obtain conformer-specific UV spectra using IR–UV hole-burning spectroscopy. The results, shown in Figure 3, show a close similarity between the four spectra, which are all dominated by their respective  $S_0$ – $S_1$  origin transitions, with weak Franck–Condon activity in one or more low-frequency fundamentals of about 25 cm<sup>-1</sup>.

3.2.3. IRPT Spectra: Fractional Abundances of  $\gamma^4 F$ . IRPT spectroscopy can be used to measure the fractional abundances of each conformer in the supersonic expansion. The IRPT spectrum of each conformer i in the amide NH-stretch region,  $I_i^{\text{PT}}(\tilde{\nu})$ , is shown as colored traces in Figure 5. After normalization to the R2PI ion signal in the absence of the IR laser, their vertical scale represents the fractional change in the population of the indicated conformation. Accordingly, in the IRPT spectra, values above the baseline signify a gain in population, while values below the baseline correspond to depletion. The loss and gain of the population between conformations are readily apparent, particularly in the spectra of conformers A and D. The black trace shown at the top of Figure 5 is the weighted sum of all the IRPT spectra (see eq 1), where the weighting factors for each IRPT spectra used in the sum are the fractional abundances  $F_i$  of each conformer i.

The IR–UV hole-filling spectra shown in Figure S5 demonstrate that collisional re-cooling of the IR-excited population is complete so that the population depleted from the zero-point vibrational level is due solely to isomerization to other conformers and not to incomplete cooling of the vibrationally excited population. Figure S5 also shows that all the population is redistributed only to conformers identified in the R2PI spectrum, meeting all conditions required to use eq 1.<sup>19</sup>

The best-fit weighted sum shown in the black trace on top is on the same vertical scale, with little deviation from zero over

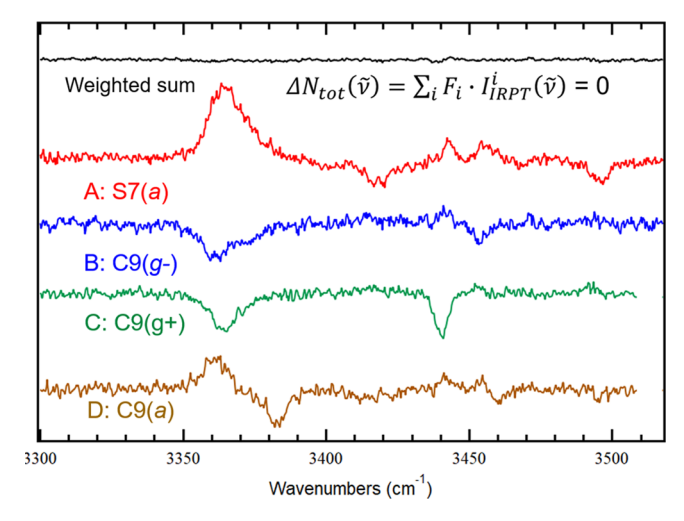


Figure 5. IRPT spectra of the four assigned conformers A–D of  $\gamma^4$ F shifted for clarity (colored). The signal above (below) the baseline corresponds to a gain (loss) of population from that conformer at that IR wavenumber. (Black, Top) Weighted sum of the IRPT spectra that minimizes the net excursion from zero at all wavelengths. The weighting coefficients are the fractional populations  $F_i$  of each conformer i in eq. 1. See the text for further discussion.

its entire wavenumber range from 3300 to 3520 cm<sup>-1</sup>. In this case, the average rms error is equivalent to the absolute value of the weighted sum averaged over all frequencies. In the best fit, this average deviation from zero is  $(2.6 \pm 1.6) \times 10^{-3}$ , a value almost a factor of 200 smaller than the maximum intensity of the weighted components (0.486). The relative populations extracted from this best fit are 53  $\pm$  5% B[C9(g-)], 27 ± 5% A[S7(a)], 13 ± 5% C[C9(a)], and 7  $\pm$  1% D[C9(a)]. In our previous study of  $\gamma^2$ F, we compared the populations obtained by IRPT spectra with those extracted from the relative intensities of the free amide NH-stretch transitions in the IR-ion gain spectrum.<sup>20</sup> While we have recorded the IR-ion gain spectrum for  $\gamma^4$ F, we have not used it to obtain fractional abundances because in  $\gamma^4$ F there is a  $\pi$ bound NH stretch and a free NH stretch of the S7(a) structure, which is partially stacked, that have calculated intensities that are quite different from the free amide NHstretch transitions, thus adding additional uncertainty to the population analysis that uses the ion-gain spectrum. Table 2 provides a summary of the \( \gamma^4 \text{F} \) percent abundances and compares them to the percent abundances in  $\gamma^2 F$  taken from Buchanan et al.20

# 4. DISCUSSION

4.1. Energy and Population Analyses of the  $\gamma^4$ F Monomer. A cursory inspection of the assigned conformers of

Table 2. Percent Populations of Ac- $\gamma^4$ -Phe-NHMe and Ac- $\gamma^2$ -Phe-NHMe Determined Using IRPT Spectroscopy

	$\gamma^2$ -Phe <sup>a</sup>	$\gamma^4$ -Phe
S7(a)	n/a	$27 \pm 5$
C9(g+)	n/a	$13 \pm 2$
C9(g-)	$41 \pm 2$	$53 \pm 5$
C9(a)	$38 \pm 1$	$7 \pm 1$
S(a)	$21 \pm 1$	n/a

<sup>&</sup>lt;sup>a</sup>From ref 20.

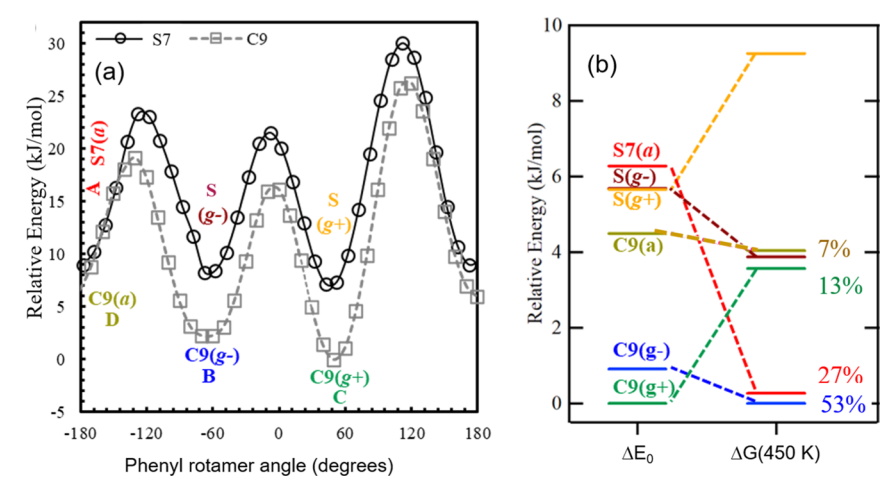


Figure 6. (a) Relaxed potential energy curves for motion about the phenyl rotor dihedral angle in  $\gamma^4 F$  starting from the S7(a) or C9(a) minima. (b) Zero-point-corrected relative energies ( $\Delta E_0$ ) and free energies ( $\Delta G$ ) of  $\gamma^4 F$  at the pre-expansion nozzle temperature of 450 K. All phenyl rotamers of C9 and stacked/S7 minima are included, including the two stacked structures not observed experimentally ((S(g-) and S(g+)). All calculations were carried out at the DFT B3LYP-GD3BJ 6-31+g(d) level of theory.

γ<sup>4</sup>F, their populations, and relative energies raises an immediate question: why are all three phenyl rotamers of the C9 structure observed but only a single phenyl rotamer of the S7 structure? We hypothesized, first, that there could be larger phenyl rotamer barriers separating the C9 structures than the S7 conformers, thereby trapping populations in all three C9 conformers during the collisional cooling process, while the S7 rotamers could isomerize and cool into the single-observed S7 minimum. To address this hypothesis, we performed relaxed potential energy scans along the phenyl rotamer dihedral angle starting from both the S7(a) and C9(a) structures. The results are shown in Figure 6a. These scans are not zero-point corrected but provide estimates of the relative energies of the S7 phenyl rotamers and the barriers to isomerization. Notably, the barriers separating the C9 conformers (10–15 kJ/mol) are similar to those involving S7 conformers, making it hard to argue on that basis for selective cooling of one relative to the other. Furthermore, the two minima in the S7 scan were calculated to be slightly lower in energy than S7(a).

Interestingly, in the S7 scan (black line), the weak, strained S7 hydrogen bond present in S7(a) is broken in the g+ and g-rotamers, producing amide-stacked configurations at these phenyl rotamer geometries. Indeed, the predicted NH-stretch transitions for the g+ and g- minima are at 3444 and 3454 cm<sup>-1</sup> separated by just 10 cm<sup>-1</sup> rather than the experimentally observed 80 cm<sup>-1</sup> splitting (3416 and 3496 cm<sup>-1</sup>). This small splitting is characteristic of the stacked configuration, as was demonstrated in the earlier studies of Ac- $\gamma^2$ -Phe-NHMe. That is result, we refer to these two minima as S(g+) and S(g-) in what follows, with structures shown in Figure S6.

An alternative hypothesis is that kinetic trapping of the preexpansion populations is occurring, wherein the observed populations are dictated by thermal equilibrium at the nozzle temperature of 450 K; that is,  $\Delta G(450 \text{ K})$ . To test this possibility, we calculated the relative free energies of the conformers at the nozzle temperature,  $\Delta G(450 \text{ K})$ , using the calculated harmonic vibrational frequencies, as shown in Figure 6b. Note that free energies substantially re-order the conformer populations compared to those one would surmise based on  $\Delta E_0$ . Furthermore, the experimental ordering of populations is reproduced by calculations, with B[C9(g-)] having the largest population, followed by A[S7(a)], C[C9(g+)], and D[C9(a)]. Quantitatively, the match-up is somewhat less satisfying in two respects. First, the calculated populations predict that C9(g-) and S7(a) should have similar populations (32 and 30%), whereas experimentally, C9(g-) has almost twice the population of S7(a). Second, the free energy calculations also predict an 11% abundance for S(g-), which was not detected in our work. These discrepancies are likely ascribed to deficiencies in the calculated relative energies at the current level of theory.

The large change in energy ordering between  $\Delta E_0$  and  $\Delta G(450~{\rm K})$  points to entropic differences between the conformers that reflect the overall rigidity of each conformer and therefore its vibrational partition function. We see that S7(a) gains population as the temperature rises, while C9(g+) loses population. While the number of low-frequency vibrations in the different conformers is similar, the eight vibrations less than  $100~{\rm cm}^{-1}$  are of a lower frequency in S7(a) than in C9(g+) for two principal reasons. First, S7(a) has a weak S7 H-bond in an almost-stacked conformation, softening the potential for motion between the two amide planes. Second, the phenyl ring plane in S7(a) points away from the almost-stacked amide planes, increasing its flexibility relative to C9(g+) with its more structurally rigid C9 H-bond and more restricted g+ phenyl ring position.

**4.2.** Conformational Preferences of  $\gamma^4F$  Compared to  $\gamma^2F$ . One of the strengths of the present work is that we have determined not only which conformations of  $\gamma^4F$  are present but also their fractional abundances derived from IRPT studies. As we have already alluded to,  $\gamma^4F$  has the phenylalanine (Phe, F) side chain positioned in the 4-position of the  $\gamma$ -peptide backbone immediately adjacent to the N-terminal amide NH. In Table 2, we have compared the fractional abundances of  $\gamma^4F$  with its close structural analogue,  $\gamma^2F$ , in which the Phe side chain is at the 2-position in the  $\gamma$ -peptide backbone adjacent to the C-terminal C=O group.

The comparison between  $\gamma$  is complicated by the notation used to define the phenyl rotamer conformations. The reader will recall that the (a, g+, and g-) designations are defined using the dihedral from the N-terminal side of the capped peptide. In  $\gamma^4$ F, this is the N-C(4)-CH<sub>2</sub>-C(ph) angle shown in red in Figure 1, while in  $\gamma^2$ F, it is the C(3)-C(2)-CH<sub>2</sub>-C(ph) dihedral. As a result, as shown in Figure 4b,  $\gamma^4$ F C9(g+)

and  $\gamma^4F$  C9(g-) place the phenyl ring in close proximity to the NH group, while  $\gamma^4F$  C9(a) is near the C(3)H<sub>2</sub>. The  $\pi$  H-bond formed between the N-terminal amide NH group and the phenyl  $\pi$  cloud stabilizes  $\gamma^4F$  C9(g+) and  $\gamma^4F$  C9(g-) relative to C9(a), leading to greater abundances of the former two over the latter. The spectroscopic manifestation of the NH  $\pi$  H-bonds is a shift to a lower frequency by 5 and 19 cm<sup>-1</sup> relative to the free NH stretch of C9(a).

In contrast, in  $\gamma^2 F$ , two C9 conformers,  $\gamma^2 F$  C9(a) and  $\gamma^2 F$  C9(g-), are observed, but  $\gamma^2 F$  C9(g+) is missing. The former two conformers place the phenyl ring well away from the C-terminal C=O group, while C9(g+) is not observed because in that case the phenyl ring would interact closely with the C=O group, destabilizing it relative to the other C9 minima in  $\gamma^2 F$ , which carry the majority of the population (Table 2).

The changed position of substitution of the Phe side chain also affects the amide-stacked structures of the two molecules. In  $\gamma^2 F$ , a single, "pure" stacked conformation is observed, S(a), that places the phenyl ring over the capped C-terminal amide plane. The analogous structure in  $\gamma^4 F$  is S7(a), in which the phenyl group is oriented away from the  $\gamma$ -peptide backbone where it interacts with no other groups. Since the stacked amide groups are completely unrestrained, the plane of the N-terminal amide group tips to form a weak S7 H-bond with the C-terminal C=O, with this mixed stacked/S7 structure labeled as S7(a). The reader will recall that the other two phenyl rotamers of S7  $\gamma^4 F$ , S(g+) and S(g-), are more nearly pure amide-stacked structures, consistent with the notion that the phenyl ring stabilizes the amide-stacked structures in these cases.

The structural changes that occur between  $\gamma^2 F$  S(a) and  $\gamma^4 F$  S7(a) are obvious from considering the set of peptide backbone dihedral angles shown in Table 3. Note, first, that

Table 3. Table of Dihedral Angles of Indicated  $\gamma^4 F$  and  $\gamma^2 F$  Conformers

structure	$\phi$	$ heta_1$	$ heta_2$	Ψ
γ <sup>4</sup> F C9	101	-69	-74	104
$\gamma^4$ F S7(a)	-154	63	-73	147
$\gamma^2 F S(a)^a$	-102	55	-76	136
$\gamma^2 F C9^a$	99	-70	-73	105

<sup>a</sup>Taken from ref 20.

three of the four dihedrals are nearly identical, with the  $\phi$  dihedral (Figure 1) that controls the relative orientation of N-terminal amide plane as the only angle that changes significantly. This change is induced by the position of the phenyl ring in  $\gamma^2 F$  S(a) relative to  $\gamma^4 F$  S7(a). The antiorientation of the phenyl ring points it out and away from the backbone in  $\gamma^4 F$  but over the amide stack in  $\gamma^2 F$ . The interaction of the phenyl ring with the amide  $\pi$ -cloud stabilizes the amide stack in a nearly anti-parallel arrangement in  $\gamma^2 F$ , with the same amide group re-orienting to form a weak S7 H-bond in the absence of that stabilization.

The structural similarities between the pure-stacked structure S(a) found in both  $\gamma$  molecules funnel the majority of their population into C9 conformations (73% in  $\gamma^4$ F and 79–83% in  $\gamma^2$ F), with the distribution between phenyl rotamers dictated by a combination of enthalpic and entropic contributions associated with the attraction of the phenyl ring for the adjacent NH group in  $\gamma^4$ F and the avoidance of the C=O by the phenyl ring in  $\gamma^2$ F. Both molecules also support a

significant population in a single amide-stacked-like structure, either S(a) or S7(a). There is a somewhat greater population in  $\gamma^4F$  S7(a) than in  $\gamma^2F$  S(a), but this difference is near the error limits (Table 2).

One intriguing and unresolved question raised by the data is the very different intensity ratios of the amide-stacked and C9 conformers in the R2PI spectra of  $\gamma^4$ F relative to  $\gamma^2$ F, as shown in Figure S7. In  $\gamma^4$ F, the S7(a) and C9(g–) conformers have a population ratio of 1:2 but an intensity ratio in the R2PI spectrum of 1:1. This difference could easily be understood as being due to differences in Franck–Condon factors or photoionization efficiencies between the conformers. In contrast, the S(a) and C9(g–) conformers of  $\gamma^2$ F have a population ratio of 1:2 but an R2PI intensity ratio of 1:10. This striking difference may be due to conformation-specific fragmentation following photoionization (see Figure S2). If so, it was not identified in the previous work 17 and would be interesting to explore.

**4.3. IR-Induced Isomerization.** IR population transfer studies such as those described here on  $\gamma^4 F$  not only determine the fractional abundances of the conformers but also demonstrate whether IR-induced isomerization is possible and efficient between all observed conformers. In order to gain a deeper understanding of this data, it is important to have predictions not only for the relative energies and free energies of the conformers but also for the conformational landscape that includes the barriers to isomerization and the pathways that connect them.

Disconnectivity graphs provide a useful and visually intuitive summary of the potential energy landscape for conformational isomerization. <sup>13,55</sup> Individual branches on the graph end at energies associated with the calculated relative energies of conformational minima, while transition states connecting the minima below them are grouped into user-defined energy windows (1 kcal/mol in this case) and visualized as branching points on the graph. Figure 7 presents the disconnectivity graphs for  $\gamma^4 F$  calculated using the AMBER\* force field. While force fields can have systematic errors when applied to synthetic foldamers with their non-standard functional groups, in the case of  $\gamma^4 F$  and  $\gamma^2 F$ , the predicted low-energy conformers account for observations remarkably well. For

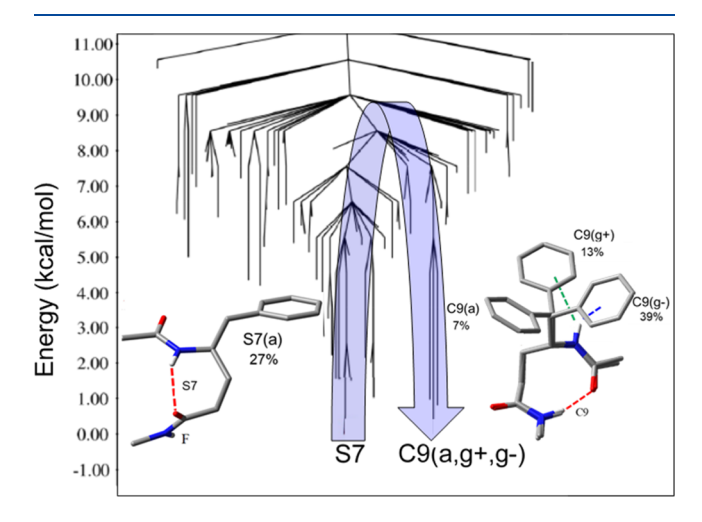


**Figure 7.** Disconnectivity graph for  $\gamma^4F$  created using the AMBER\* force field. The arrow shows the pathway for selective IR excitation of the S7(a) conformer via an NH-stretch fundamental, as carried out experimentally.

instance, the disconnectivity graph for  $\gamma^4 F$  (Figure 7) has a set of three C9 conformers that are within 1 kcal/mol and are phenyl rotamers of one another, in keeping with the observation of all three C9 phenyl rotamers in our experiment. Furthermore, a single S7-like stacked conformer of  $\gamma^4 F$  is calculated to be close in energy to the C9 conformers but exists in a different funnel on the potential energy landscape. Similarly, in  $\gamma^2 F$  (Figure S8), there are two low-energy C9 conformers with the third pushed up in energy where little populations would be anticipated to reside, with a single amide-stacked conformation being the next lowest in energy, again as observed.

Given this good correspondence between the experimental populations and the relative energies calculated by the forcefield, we use the data from the disconnectivity graph to extract the lowest energy pathway for isomerization between the various observed conformers. Not unexpectedly, the barriers connecting the various C9 phenyl rotamers are relatively small (<5 kcal/mol) and significantly below the 8–9 kcal/mol rate-limiting barriers for isomerizing between the fully or partially stacked structures and the C9 minima. The IR population transfer experiments involve IR excitation of single conformers with well-defined single-photon IR energies of 9.5–10.0 kcal/mol associated with the NH-stretch fundamentals of the two amide groups of each conformer.

Experimentally, we observe IR-induced isomerization (see Figure 5) between all three of the C9 conformers B–D. This is most clearly demonstrated by the significant gain in population of conformer D following excitation of the C9 H-bonded NH-stretch fundamentals of conformers B and C at 3360 cm<sup>-1</sup>. Similarly, the dip in conformer C population at 3440 cm<sup>-1</sup> has corresponding gains in conformers B and D, while excitation of the free amide NH-stretch of B at 3453 cm<sup>-1</sup> produces small gains in the other three conformers. Experimental observation of these isomerization processes is consistent with a barrier for interconversion of the C9 phenyl rotamers well below the excitation energy.

The more interesting process is the isomerization pathway that interconverts the  $\gamma$ -peptide backbone between the C9 and the amide-stacked-like S7(a) minimum. As the disconnectivity graph in Figure 7 shows pictorially, the S7 and C9 minima exist in two different basins on the conformational energy landscape, in this sense, mimicking circumstances in which misfolding pathways exist in proteins. That the C9  $\rightarrow$  S7 isomerization is energetically feasible is immediately evident from the large and broad gain signal in S7(a) stretching over the 3355–3390 cm<sup>-1</sup> region where the absorptions due to the H-bonded NH-stretch fundamental of the three C9 conformers of  $\gamma^4$ F occur. The reverse process, namely, excitation of S7(a) to form C9 products, is harder to detect, but the dip in population of S7(a) at 3496 cm<sup>-1</sup> does lead to a small gain, particularly in conformer C, the C9(g+) conformer.

One could argue that the gain signals out of S7(a) should be more clearly observed, particularly from the weak S7 H-bonded NH stretch at 3417 cm<sup>-1</sup>. Interestingly, the disconnectivity graph in Figure 7 shows that the rate-limiting barrier height for  $S7 \leftrightarrow C9$  isomerization is near 10 kcal/mol  $(3500 \text{ cm}^{-1})$ , an energy right in the vicinity of the IR photon energy. Indeed, this could be the reason that the  $S7 \rightarrow C9$  isomerization is so small following excitation of S7 at S7 at S7 is mediated to exceed the barrier, and re-cooling of these two photon-excited molecules may not be complete.

#### 5. CONCLUSIONS

γ-Peptides are unique among synthetic foldamers in making possible an arrangement in which adjacent amide groups form an anti-parallel, stacked configuration with no intramolecular H-bond that competes for population with H-bonded conformations. We have studied the single-conformation spectroscopy of Ac- $\gamma^4$ -Phe-NHMe ( $\gamma^4$ F) in order to compare it with the corresponding isomer in which Phe is substituted at the 2-position adjacent to the C-terminal amide C=O group  $(\gamma^2 F)$ . We characterized a set of four conformers of  $\gamma^4 F$  in the gas-phase using IR-UV double resonance methods. A unique, partially stacked conformation is found in  $\gamma^4$ F that is distorted away from parallel amide planes to facilitate the formation of a weak C7 H-bond, which we label as S7. Additionally, all three phenyl rotamers of a conformational family that possess a ninemembered H-bonded ring (labeled C9) were observed. IRPT spectroscopy was used to determine fractional abundances of the four conformers. These fractional abundances correlate well with the relative free energies of the conformers at the preexpansion nozzle temperature (450 K), indicating that kinetic trapping plays a role in the observed populations. We explored the potential energy landscape for isomerization by calculating the disconnectivity graph for  $\gamma^4 F$  and  $\gamma^2 F$  and observed that in both molecules, the amide-stacked and C9 conformers are separated by a barrier of about 10 kcal/mol, with the potential energy landscape mimicking a misfolding pathway in larger peptides and proteins.

## ASSOCIATED CONTENT

# Supporting Information

The Supporting Information is available free of charge at https://pubs.acs.org/doi/10.1021/acs.jpca.2c00112.

R2PI spectra in the presence and absence of water; TOF mass spectra showing fragmentation following photoionization; R2PI in parent and fragment mass channels; comparison of observed IR spectra with a broader range of calculated conformations; IR–UV hole-filling spectra; comparison of stacked conformers of different phenyl rotamers; comparison of R2PI spectra of  $\gamma^4$ F with  $\gamma^2$ F; disconnectivity graph for  $\gamma^2$ F; synthesis and characterization data for  $\gamma^4$ F (PDF)

# AUTHOR INFORMATION

# **Corresponding Author**

Timothy S. Zwier — Department of Chemistry, Purdue University, West Lafayette, Indiana 47907-2084, United States; Gas Phase Chemical Physics, Sandia National Laboratories, Livermore, California 94550, United States; orcid.org/0000-0002-4468-5748; Email: tszwier@sandia.gov

# **Authors**

Joshua L. Fischer – Department of Chemistry, Purdue University, West Lafayette, Indiana 47907-2084, United States

Karl N. Blodgett – Department of Chemistry, Purdue University, West Lafayette, Indiana 47907-2084, United States; © orcid.org/0000-0002-6827-0328

Christopher P. Harrilal — Department of Chemistry, Purdue University, West Lafayette, Indiana 47907-2084, United States; Present Address: Biological Sciences Division,

- Pacific Northwest National Laboratory, Richland, Washington 99354, United States
- Patrick S. Walsh Department of Chemistry, Purdue University, West Lafayette, Indiana 47907-2084, United States; Present Address: University of Dayton Research Institute, Dayton, OH 45469 United States.
- Zachary S. Davis Department of Chemistry, Wofford College, Spartanburg, South Carolina 29303, United States Sunglim Choi — Department of Chemistry, Yonsei University, Seoul 03722, South Korea
- Soo Hyuk Choi Department of Chemistry, Yonsei University, Seoul 03722, South Korea; orcid.org/0000-0003-4066-6504

Complete contact information is available at: https://pubs.acs.org/10.1021/acs.jpca.2c00112

#### **Notes**

The authors declare no competing financial interest.

# ACKNOWLEDGMENTS

J.L.F., K.N.B., C.P.H., P.S.W., and T.S.Z. gratefully acknowledge support for this work from the National Science Foundation under grant NSF CHE-1764148 while at Purdue University. S.C. and S.H.C. acknowledge support from the National Research Foundation of Korea (NRF-2021R1A2C1013477). T.S.Z. acknowledges support from the U.S. DOE Basic Energy Sciences during article preparation at Sandia. Sandia National Laboratories is a multi-mission laboratory managed and operated by the National Technology and Engineering Solutions of Sandia, LLC., a wholly owned subsidiary of Honeywell International, Inc., for the U.S. DOE National Nuclear Security Administration under contract DE-NA0003525. This paper describes objective technical results and analysis. Any subjective views of opinions that might be expressed in the paper do not necessarily represent the views of the U.S. Department of Energy or the United States Government.

# REFERENCES

- (1) Herschlag, D.; Pinney, M. M. Hydrogen Bonds: Simple after All? *Biochemistry* **2018**, *57*, 3338–3352.
- (2) Newberry, R. W.; Raines, R. T. Secondary Forces in Protein Folding. ACS Chem. Biol. 2019, 14, 1677-1686.
- (3) Zhou, H.-X.; Pang, X. Electrostatic Interactions in Protein Structure, Folding, Binding, and Condensation. *Chem. Rev.* **2018**, *118*, 1691–1741.
- (4) Dill, K. A. Dominant forces in protein folding. *Biochem* **1990**, 29, 7133–7155
- (5) Gellman, S. H. Foldamers: A manifesto. Acc. Chem. Res. 1998, 31, 173-180.
- (6) Martinek, T. A.; Fülöp, F. Peptidic foldamers: ramping up diversity. *Chem. Soc. Rev.* **2012**, *41*, 687–702.
- (7) Rinaldi, S. The Diverse World of Foldamers: Endless Possibilities of Self-Assembly. *Molecules* **2020**, *25*, 3276.
- (8) Cheng, R. P.; Gellman, S. H.; DeGrado, W. F. beta-peptides: From structure to function. *Chem. Rev.* **2001**, *101*, 3219–3232.
- (9) Bouillère, F.; Thétiot-Laurent, S.; Kouklovsky, C.; Alezra, V. Foldamers containing gamma-amino acid residues or their analogues: structural features and applications. *Amino Acids* **2011**, 41, 687–707.
- (10) Seebach, D.; Beck, A. K.; Bierbaum, D. J. The world of betaand gamma-peptides comprised of homologated proteinogenic amino acids and other components. *Chem. Biodiversity* **2004**, *1*, 1111–1239.
- (11) Seebach, D.; Hook, D. F.; Glättli, A. Helices and other secondary structures of beta- and gamma-peptides. *Biopolymers* **2006**, 84, 23–37.

- (12) Baquero, E. E.; James, W. H.; Choi, S. H.; Gellman, S. H.; Zwier, T. S. Single-conformation ultraviolet and infrared spectroscopy of model synthetic foldamers: beta-peptides Ac-beta(3)-hPhe-NHMe and Ac-beta(3)-hTyr-NHMe. *J. Am. Chem. Soc.* **2008**, *130*, 4784–4794
- (13) Blodgett, K. N.; Zhu, X.; Walsh, P. S.; Sun, D.; Lee, J.; Choi, S. H.; Zwier, T. S. Conformer-Specific and Diastereomer-Specific Spectroscopy of alpha beta alpha Synthetic Foldamers: Ac-Alabeta(ACHC)-Ala-NHBn. *J. Phys. Chem. A* **2018**, *122*, 3697–3710.
- (14) James, W. H.; Baquero, E. E.; Shubert, V. A.; Choi, S. H.; Gellman, S. H.; Zwier, T. S. Single-Conformation and Diastereomer Specific Ultraviolet and Infrared Spectroscopy of Model Synthetic Foldamers: alpha/beta-Peptides. J. Am. Chem. Soc. 2009, 131, 6574–6590
- (15) James, W. H.; Buchanan, E. G.; Guo, L.; Gellman, S. H.; Zwier, T. S. Competition between Amide Stacking and Intramolecular H Bonds in gamma-Peptide Derivatives: Controlling Nearest-Neighbor Preferences. *J. Phys. Chem. A* **2011**, *115*, 11960–11970.
- (16) James, W. H.; Buchanan, E. G.; Müller, C. W.; Dean, J. C.; Kosenkov, D.; Slipchenko, L. V.; Guo, L.; Reidenbach, A. G.; Gellman, S. H.; Zwier, T. S. Evolution of Amide Stacking in Larger gamma-Peptides: Triamide H-Bonded Cycles. *J. Phys. Chem. A* **2011**, *115*, 13783–13798.
- (17) James, W. H., III; Müller, C. W.; Buchanan, E. G.; Nix, M. G. D.; Guo, L.; Roskop, L.; Gordon, M. S.; Slipchenko, L. V.; Gellman, S. H.; Zwier, T. S. Intramolecular Amide Stacking and Its Competition with Hydrogen Bonding in a Small Foldamer. *J. Am. Chem. Soc.* **2009**, *131*, 14243–14245.
- (18) Walsh, P. S.; Kusaka, R.; Buchanan, E. G.; James, W. H.; Fisher, B. F.; Gellman, S. H.; Zwier, T. S. Cyclic Constraints on Conformational Flexibility in gamma-Peptides: Conformation Specific IR and UV Spectroscopy. *J. Phys. Chem. A* **2013**, *117*, 12350–12362.
- (19) Zwier, T. S. Laser probes of conformational isomerization in flexible molecules and complexes. *J. Phys. Chem. A* **2006**, *110*, 4133–4150.
- (20) Buchanan, E. G.; James, W. H., III; Gutberlet, A.; Dean, J. C.; Guo, L.; Gellman, S. H.; Zwier, T. S. Single-conformation spectroscopy and population analysis of model gamma-peptides: New tests of amide stacking. *Faraday Discuss.* **2011**, *150*, 209–226.
- (21) Hanessian, S.; Luo, X.; Schaum, R.; Michnick, S. Design of secondary structures in unnatural peptides: Stable helical gammatetra-, hexa-, and octapeptides and consequences of alphasubstitution. *J. Am. Chem. Soc.* **1998**, *120*, 8569–8570.
- (22) Seebach, D.; Brenner, M.; Rueping, M.; Jaun, B. gamma(2)-, gamma(3)-, and gamma(2,3,4)-amino acids, coupling to gamma-hexapeptides: CD spectra, NMR solution and X-ray crystal structures of gamma-peptides. *Chem.—Eur. J.* **2002**, *8*, 573–584.
- (23) Seebach, D.; Brenner, M.; Rueping, M.; Schweizer, B.; Jaun, B. Preparation and determination of X-ray-crystal and NMR-solution structures of gamma(2,3,4)-peptides. *Chem. Commun.* **2001**, *2*, 207–208.
- (24) Zwier, T. S. The spectroscopy of solvation in hydrogen-bonded aromatic clusters. *Annu. Rev. Phys. Chem.* **1996**, *47*, 205–241.
- (25) Dian, B. C.; Florio, G. M.; Clarkson, J. R.; Longarte, A.; Zwier, T. S. Infrared-induced conformational isomerization and vibrational relaxation dynamics in melatonin and 5-methoxy-N-acetyl tryptophan methyl amide. *J. Chem. Phys.* **2004**, *120*, 9033–9046.
- (26) Dian, B. C.; Longarte, A.; Winter, P. R.; Zwier, T. S. The dynamics of conformational isomerization in flexible biomolecules. I. Hole-filling spectroscopy of N-acetyl tryptophan methyl amide and N-acetyl tryptophan amide. *J. Chem. Phys.* **2004**, *120*, 133–147.
- (27) Harrilal, C. P.; DeBlase, A. F.; Fischer, J. L.; Lawler, J. T.; McLuckey, S. A.; Zwier, T. S. Infrared Population Transfer Spectroscopy of Cryo-Cooled Ions: Quantitative Tests of the Effects of Collisional Cooling on the Room Temperature Conformer Populations. J. Phys. Chem. A 2018, 122, 2096–2107.
- (28) Harder, E.; Damm, W.; Maple, J.; Wu, C.; Reboul, M.; Xiang, J. Y.; Wang, L.; Lupyan, D.; Dahlgren, M. K.; Knight, J. L.; et al. OPLS3:

- A Force Field Providing Broad Coverage of Drug-like Small Molecules and Proteins. J. Chem. Theory Comput. 2016, 12, 281–296.
- (29) Weiner, P. K.; Kollman, P. A. AMBER: Assisted model building with energy refinement. A general program for modeling molecules and their interactions. *J. Comput. Chem.* **1981**, *2*, 287–303.
- (30) Lee, C.; Yang, W.; Parr, R. G. Development of the Colle-Salvetti Correlation Energy Formula into a Functional of the Electron Density. *Phys. Rev. B* **1988**, *37*, 785–789.
- (31) Goerigk, L.; Kruse, H.; Grimme, S. Benchmarking Density Functional Methods against the S66 and S66x8 Datasets for Non-Covalent Interactions. *ChemPhysChem* **2011**, *12*, 3421–3433.
- (32) Grimme, S.; Antony, J.; Ehrlich, S.; Krieg, H. A consistent and accurate ab initio parametrization of density functional dispersion correction (DFT-D) for the 94 elements H-Pu. *J. Chem. Phys.* **2010**, 132, 154104.
- (33) Zhao, Y.; Truhlar, D. G. Density functionals for noncovalent interaction energies of biological importance. *J. Chem. Theory Comput.* **2007**, *3*, 289–300.
- (34) Frisch, M. J.; Trucks, G. W.; Schlegel, H. B.; Scuseria, G. E.; Robb, M. A.; Cheeseman, J. R.; Scalmani, G.; Barone, V.; Petersson, G. A.; Nakatsuji, H.; Li, X.; et al. *Gaussian 16*, Rev. C.01: Wallingford, CT, 2016.
- (35) Evans, D. A.; Wales, D. J. Free energy landscapes of model peptides and proteins. *J. Chem. Phys.* **2003**, *118*, 3891–3897.
- (36) Mohamadi, F.; Richards, N. G. J.; Guida, W. C.; Liskamp, R.; Lipton, M.; Caufield, C.; Chang, G.; Hendrickson, T.; Still, W. C. MACROMODEL An Integrated Software System for modeling Organic and Bioorganic molecules using Molecular Mechanics. *J. Comput. Chem.* 1990, 11, 440–467.
- (37) Fredericks, S. Y.; Jordan, K. D.; Zwier, T. S. Theoretical characterization of the structures and vibrational spectra of benzene—(H2O) n (n= 1– 3) clusters. *J. Phys. Chem.* **1996**, *100*, 7810–7821.
- (38) Garrett, A. W.; Zwier, T. S. Multiphoton Ionization Studies of Clusters of Immiscible Liquids 2.  $C_6H_6$ - $(H_2O)_n$ , n=3-8 and  $(C_6H_6)_2$ - $(H_2O)_{1,2}$ . *J. Chem. Phys.* **1992**, *96*, 3402–3410.
- (39) Gotch, A. J.; Zwier, T. S. Multiphoton Ionization Studies of Clusters of Immiscible Liquids 1.  $C_6H_6$ - $(H_2O)_n$ , n=1,2. *J. Chem. Phys.* 1992, 96, 3388–3401.
- (40) Baquero, E. E.; James, W. H.; Choi, S. H.; Gellman, S. H.; Zwier, T. S. Single-conformation ultraviolet and infrared spectroscopy of model synthetic foldamers: beta-peptides Ac-beta(3)-hPhe-beta(3)-hAla-NHMe and Ac-beta(3)-hAla-beta(3)-hPhe-NHMe. *J. Am. Chem. Soc.* 2008, 130, 4795–4807.

# **□** Recommended by ACS

Coexistence of Left- and Right-Handed 12/10-Mixed Helices in Cyclically Constrained β-Peptides and Directed Formation of Single-Handed Helices upon Si...

Karl N. Blodgett, Timothy S. Zwier, et al.

JUNE 04, 2020

THE JOURNAL OF PHYSICAL CHEMISTRY A

DEAD E

Collection and Characterization by Mass Spectrometry of the Neutral Serine Octamer Generated upon Sublimation

Rong Chen, R. Graham Cooks, et al.

DECEMBER 10, 2020

ANALYTICAL CHEMISTRY

READ **C** 

Unidirectional Double- and Triple-Hydrogen Rearrangement Reactions Probed by Infrared Ion Spectroscopy

Dennis Zeh, Dietmar Kuck, et al.

APRIL 26, 2022

JOURNAL OF THE AMERICAN SOCIETY FOR MASS SPECTROMETRY

READ 🗹

Tackling a Curious Case: Generation of Charge-Tagged Guanosine Radicals by Gas-Phase Electron Transfer and Their Characterization by UV-vis Photodissociation...

Yue Liu, František Tureček, et al.

FEBRUARY 10, 2021

JOURNAL OF THE AMERICAN SOCIETY FOR MASS SPECTROMETRY

READ 🗹

Get More Suggestions >